Finite Element Analysis of Low-Intensity Laser Heating in Gold::Vanadium Dioxide Nanocomposites

by

Evan R. MacQuarrie

Advisor:

Dr. Richard F. Haglund, Jr.

Submitted to the Department of Physics and Astronomy at Vanderbilt University in partial fulfillment of the requirements for an Honors Degree in Physics

to be awarded on

May 13, 2011

VANDERBILT UNIVERSITY

ABSTRACT

Finite element modeling was performed using COMSOL Multiphysics to study the thermal dynamics of gold::vanadium dioxide (VO_2) nanocomposites. These simulations were done to understand the data from transient absorption pump probe measurements taken over the previous two years by the author. The various parameters contributing to the dynamics of the system were systematically varied within the simulation in order to understand how the various properties of the nanocomposite affect the thermodynamics of the system. It was determined that the background temperature and the optical properties of the film make the dominant contributions to the system response. The simulation was able to predict the maximum change in transmission measured in experiment fairly well but could not predict the speed at which the system responded to the pump laser. Steps to improve upon the agreement between experiment and simulation are proposed.

Keywords: Finite element analysis, vanadium dioxide, metal nanoparticles, optical limiter, plasmonic modulator

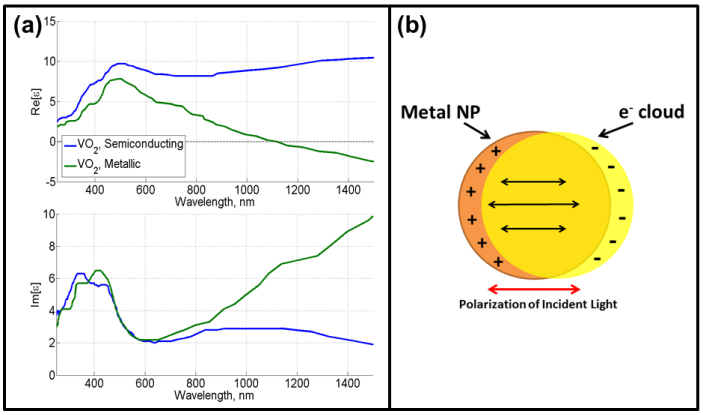

Figure 1. (a) Dielectric function of VO_2 in the semiconducting and metallic states; (b) Schematic of the oscillating electron plasma that forms an LSP.

1. INTRODUCTION

1.1 Motivation

As the applications for nanotechnology and nanophotonics grow, so does the demand for structures exhibiting dynamically tunable responses. The reversible semiconducting-to-metallic phase transition (SMT) of VO_2 is a tempting phenomenon to exploit to this end, especially when paired with the highly tunable optical properties of localized surface plasmons (LSPs) in metal nanoparticles (NPs). This idea of a NP::VO_2 nanocomposite structure is an intriguing concept since it combines both the distinct, two-state transition of VO_2 with the sensitive tunability that LSPs offer. It has therefore become necessary to form a better understanding of how NP::VO_2 nanostructures respond to stimuli that initiate the phase transition.

Since Morin first discovered the SMT of VO_2 in 1959,[1] it has attracted a significant amount of attention from the scientific community. The SMT of VO_2 is known to occur optically,[2,3] thermally ($T_c = 67°C$),[1,4] or with an applied electric field.[5] Upon transitioning into its metallic state, VO_2 experiences an abrupt change in many of its optical and thermal properties. This includes a sudden change in both the real and imaginary parts of the dielectric function of the VO_2. These changes in the dielectric function are most significant at infrared wavelengths, with little variation coming over visible wavelengths (Figure 1a). The dynamical response of VO_2 to laser irradiation is a relatively unstudied aspect of the substance, yet the laser switching of VO_2 is an attractive mechanism for a number of applications. For the low-powered laser applications that this paper is concerned with, the SMT typically occurs on a millisecond timescale due to laser heating within the material. Experiments in this regime are typically conducted to develop VO_2 as an optical limiting material, a protective coating for detectors, or as an optical switch.[6–9]

The LSPs that can be excited in metallic NPs arise from the collective, free-electron response of the NP to incident light. Such a system can be thought of as a damped-driven oscillator (DDO), with the driving force taking the form of the incident light's oscillating electric field while the damping arises from intraparticle forces (Figure 1b). Like any good DDO, LSPs exhibit a resonant absorption (LSPR), which typically comes over visible or near-infrared wavelengths

and dominates the optical spectra of the NPs. The location and shape of a LSPR is highly sensitive to such things as NP size and shape, interactions with nearby NPs, and the local dielectric function,[10–20] making them highly tunable structures that make ideal nanoantennae for detecting small changes in the local environment.[21]

The intrigue of a NP::VO_2 nanocomposite begins to develop when one couples the abrupt change in the dielectric function of transitioning VO_2 with the sensitive dependence of a NP's LSPR to the local dielectric function. By heating the VO_2 through its SMT, one can reversibly alter the structure of the LSPR of any NPs embedded within a VO_2 film, thus providing the NPs with a dynamic, two-state tunability and giving the VO_2 optically interesting properties at visible wavelengths.[22–28] In this work, we investigate the response of these NP::VO_2 nanocomposites to low-powered laser irradiation using transient absorption measurements[29] and then attempt to understand this experimental system via finite element analysis.

1.2 Experimental Motivation

Using electron beam lithography, square arrays of 140 nm diameter Au NPs with a 350 nm grating constant and 20 nm height were fabricated on indium-tin-oxide (ITO) coated silica glass substrates. VO_2 was then deposited to a depth of 60 nm on top of the NPs through the pulsed laser deposition (PLD) of a vanadium target in an oxygen background followed by annealing in oxygen background. This fabrication process is summarized in Figure 2. White light transmission measurements were then made as the VO_2 was heated and cooled through its SMT to verify the quality of the VO_2 and characterize the sample. Extinction measurements were also made on the arrays to locate the LSPRs of the NPs. Figure 3a shows that these LSPRs blueshift from 1000 nm to 850 nm as the VO_2 transitions into the metallic state.

Transient absorption pump probe measurements were then taken both on the plain VO_2 film and on the array of NPs using the experimental setup shown in Figure 3b. The sample was held at 55°C (a temperature near but just below the SMT point), and when triggered, the 785 nm pump beam irradiated the sample for 5.5 s. Over this time, the pump beam provided the necessary thermal energy to increase the sample temperture by as much as 25°C, thus increasing the fraction of VO_2 domains that had transitioned into the metallic state. This transition was observed as a decrease in the transmission of a 1550 nm probe beam that had been focused to the same point on the sample as the pump beam. Contrast was then defined as the ratio of the probe transmission as a function of time to the probe transmission before the pump beam was triggered: $C(t) = \tau(t)/\tau_0 - 1$. Here we have subtracted 1 simply to zero the initial contrast and make the plots more intuitive to read. A decrease in contrast should be interpreted as a decrease in probe transmission. This process was repeated for several different pump intensities, and these results are shown in Figure 4a.

Because VO_2 switches via percolation, its transition behavior maps to a sigmoid. Noting this, maximum contrast was plotted as a function of incident intensity (Figure 4b) and fit with the three-parameter sigmoid given by Equation 1 where I_c is the critical intensity at which the transition sigmoid is centered, I_w is the width of the sigmoid, and C_M is, according to the fit, the maximum contrast that would be achieved when VO_2 is fully transitioned into the metallic state. From this fit, the threshold intensity needed to induce the SMT was extracted for both

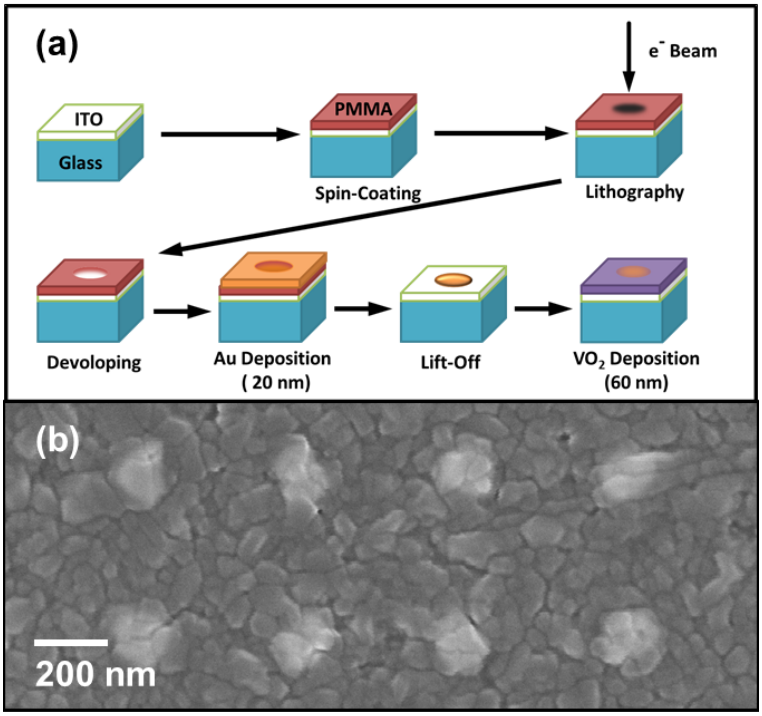

Figure 2. (a) Fabrication process; (b) SEM image of 140 nm diameter Au NPs underneath a 60 nm VO_2 film.

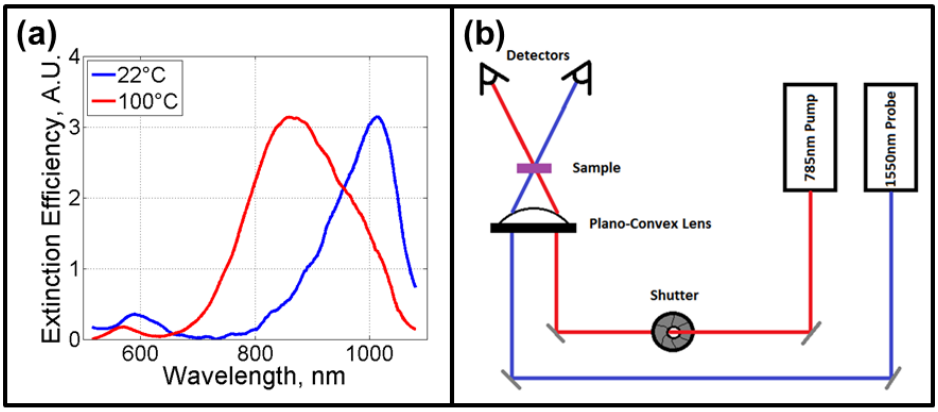

Figure 3. (a) Extinction spectra for Au::VO_2 nanocomposite; (b) Experimental setup for the transient absorption pump probe measurements.

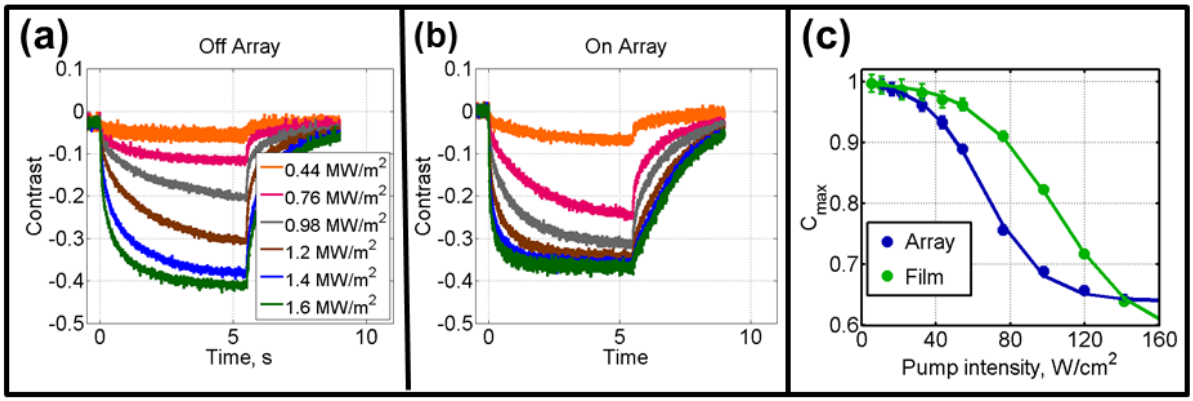

Figure 4. Contrast vs. time plots both (a) on the plain film and (b) on the nanocomposite; (b) Contrast plotted as a function of incident intensity and fit with a sigmoid, both for the plain VO_2 film and the nanocomposite.

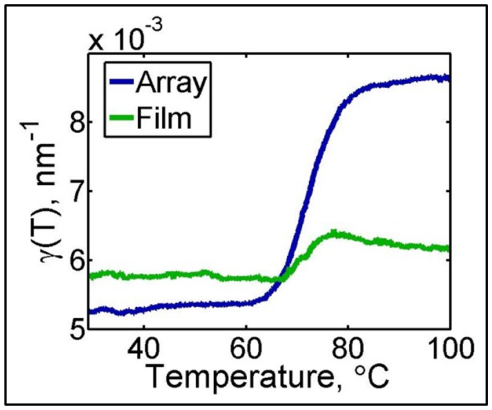

Figure 5. Absorption constant of both the plain VO_2 film and the Au::VO_2 nanocomposite as calculated from transmission measurement data.

the film and the nanocomposite. It was found that even when Au NPs constitute only 4% by volume of the nanocomposite they are able to reduce the threshold intensity by up to 37% and the time to complete the SMT by a factor of ≈ 5. It is thought that the NPs accomplish this by acting as both 'nanoradiators' that scatter light back into the film and absorption centers that capture the incident energy more efficiently. Both of these mechanisms act to increase the fraction of incident light that is absorbed within the film, and this can be modeled by a change in the effective absorption constant for the nanocomposite as compared to the plain film. The effective absorption constant γ_{eff} of the nanocomposite as a function of temperature was extracted from the transmission measurements taken to verify VO_2 film quality. The results are shown in Figure 5.

$$C(I) = 1 - \frac{1 - C_M}{1 + \exp\left[-\frac{I - I_c}{I_w}\right]} \tag{1}$$

Experiment has thus shown that the presence of NPs beneath a VO_2 film alters the macro-

	$VO_{2,semi}$	$VO_{2,met}$	Au::$VO_{2,semi}$	Au::$VO_{2,met}$
Density, ρ [g/cm^3]	4.65	4.65	4.65	4.65
Absorption Constant ($\lambda = 785$ nm), γ [m^{-1}]	5.8×10^6	6.1×10^6	5.3×10^6	8.7×10^6
Reflectivity, R	0.25	0.17	0.25	0.17
Thermal Conductivity, κ [W/mK]	3.5	5.8	3.5	5.8
Heat Capacity, C_p [J/kgK]	645	774	645	774

Table 1. Material properties used for simulating VO_2.

scopic properties of the film. To fully understand these nanocomposite systems, however, it is necessary to create a computational model for the experimental system that reproduces the observed behavior. By doing so, it will be possible to observe the effect each aspect of the nanocomposite has on its behavior, thereby establishing a more robust understanding of these structures and guiding the fabrication of the next generation of nanocomposites.

2. METHODOLOGY

Numerical simulations were done using the COMSOL Multiphysics Heat Transfer module, which uses finite element analysis to solve the heat equation. Exploiting the cylindrical symmetry of the problem, the simulation was constructed on a two-dimensional plane with positive radial values extending away from the center of the beam spot.

The substrate was defined as a 500 μm by 1 mm rectangle of silica glass, with the material properties given in the COMSOL Material Library. On top of this, a 60 nm by 1 mm rectangle was placed to represent the VO_2 film. VO_2 is not included in the COMSOL Material Library so its optical properties were estimated from experimental measurements while its other properties were taken from the literature.[30] These properties are summarized in Table 1. Inside of this film, a subregion was defined from $r = 0$ to $r = 3R_s$ where R_s is defined as the radius of the spot, which was measured by a knife-edge experiment to be 121 μm. In this region, the Gaussian heat source given by Equation 2 was defined where R is the reflectivity at the surface of the VO_2 film, I_0 is the intensity incident on the sample, and γ is the absorption constant of the film. The Gaussian envelope in Equation 2 was determined from the knife-edge measurements.[31] The simulation region is depicted in Figure 6.

$$Q(r,z) = (1-R)I_0\gamma\ e^{-\gamma z}e^{-\frac{r^2 ln(2)}{R_s^2}} \tag{2}$$

The phase transition of the VO_2 was taken into account by defining sigmoidal changes in the parameters defining the relevant optical (absorption constant and reflectivity) and thermal (thermal conductivity and heat capacity) properties of the VO_2 film. These sigmoidal changes are given in a generalized form by Equation 3 where α is a generic property of the film, T_t is the transition temperature of the film, and T_w is the width of the sigmoidal transition. T_t and T_w are set to 66.8°C and 3.50°C respectively for simulations comparing simulation to experiment and 72°C and 2.75°C when doing general parametric investigations. The values used when

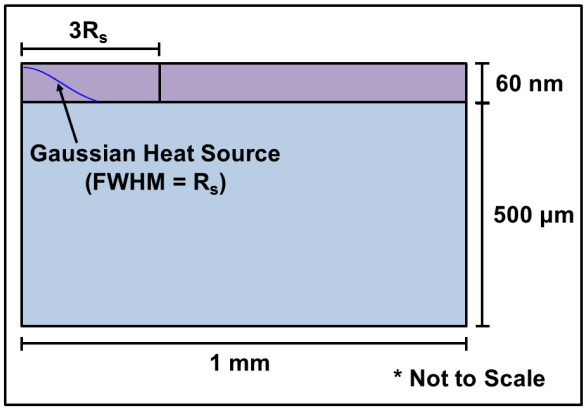

Figure 6. The geometric structure of our simulations.

comparing simulations to experiment were extracted from a sigmoidal fit to the transmission hysteresis obtained by heating the experimental sample through its SMT, while the second set of constants represent more typical values for a VO_2 film. Although VO_2 switches through the percolation of individual domains, mean field theory allows the varied local properties to be treated together with an average over the aggregate properties of the film. This justifies treating the SMT as a sigmoidal variation in the average properties of the film.

$$\alpha(T) = \alpha_{semi}\frac{1}{1+exp(\frac{T-T_t}{T_w})} + \alpha_{met}(1-\frac{1}{1+exp(\frac{T-T_t}{T_w})}) \tag{3}$$

When simulating the Au::VO_2 nanocomposites, the only change that was made to the simulation was replacing the absorption constant of the film with the experimentally determined effective absorption constant for the nanocomposite given in Table 1. The reflectivity also changes for the nanocomposite as compared to the plain film, but the measured reflectivity of the nanocomposite was not available so this was not taken into account.

Boundary conditions were then defined at the appropriate interfaces. A thin thermally resistive layer was added between the VO_2 film and the silica glass substrate to model thermal contact resistance between the two domains. This thin layer was given an effective thickness of 5 nm (on the order of the roughness thought to exist at the boundary due to the granularity of the VO_2 film) and a thermal conductance of 1 W/(m·K).[30] By varying the size of this thin layer and its conductance and by comparing these simulations with simulations run without the thin resistive layer, it was concluded that the thermal contact resistance at the interface of the two domains has a negligible effect on the response of the system. The initial temperature in each domain was set to $T_0 = 55°C$, and the boundary of the silica glass substrate that interfaces with the copper sample holder was locked to that same constant temperature $T_0 = 55°C$. This served as the ambient temperature for the simulations. Convective cooling was added at boundaries interfacing with air, but comparison with simulations lacking convection showed that convective cooling also contributes little to the system response.

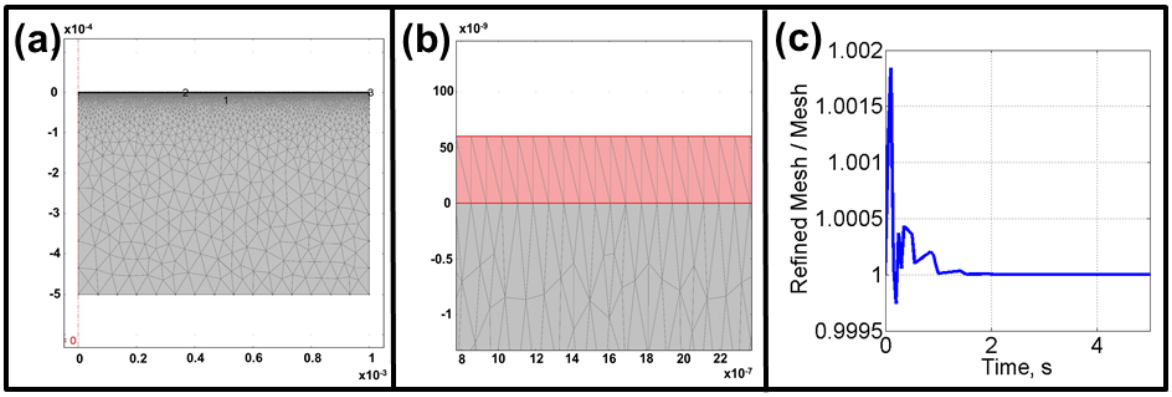

Figure 7. The mesh distribution (a) in the substrate and (b) in the portion of the VO_2 film; (c) Ratio of the temperature at a point in the film calculated with a refined mesh to the temperature at that same point calculated with the looser mesh.

In a finite element simulation, the simulation region is meshed into small elements, the intersections of which define the points at which the PDE's governing the problem are solved. COMSOL's Free Triangular meshing scheme was implemented, which divides each domain into a series of triangular elements. The resulting mesh is shown in Figure 7. To test the numerical stability of the simulation, the mesh was then refined using COMSOL's 'Refine Mesh' command twice. Every time it is called, this command divides each mesh element into four smaller regions of equal area. After these refinements, the density of elements within the VO_2 film had increased by a factor of 50, yet the simulation results changed by a negligibly small amount within the film (Figure 7c) and the temperature distribution within the substrate was visually identical. This shows that the specific dynamics within the film are largely inconsequential, and it justifies the use of mean field theory as a means to treat the aggregate properties of the film as simply the average of the local properties within the film.

The temperature distribution of the sample was then calculated every 0.05 s for 5.3 s. A typical distribution is shown in Figure 8. To analyze the dynamics of the system, we took the point in the middle of the film at $r = 0$ m and plotted its temperature as a function of time. Equation 4 allowed us to convert the resulting plot into a plot of contrast versus time, which we could then compare with our experimental results.

$$C(t) = C_M - 1 + \frac{1 - C_M}{1 + exp(\frac{T(t) - T_t}{T_w})} \tag{4}$$

3. RESULTS AND DISCUSSION

The first task for the newly developed simulation was to study what effect the various parameters have on the system. The background temperature, T_0, was examined first since it was thought that the construction of the sample holder used during the experiment might have introduced some error into the measured temperature of the sample. The sample was held on the copper

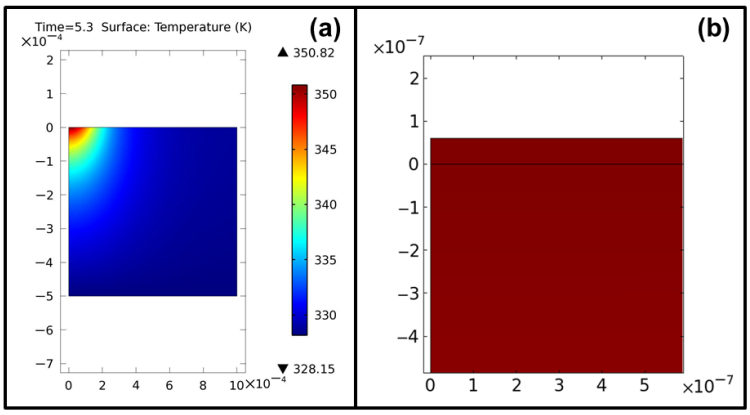

Figure 8. A typical temperature distribution in both (a) the full simulation region and (b) the film.

sample holder pictured in Figure 9a, which was heated from below by a Peltier-effect cooler working in reverse. Midway between the heat source and the sample was a glass witness slide of approximately the same thickness as the substrate of the sample. A thermocouple was attached to this witness slide, and it was here that the temperature of the sample was measured. Because the majority of the sample holder surface is exposed to air at room temperature, a thermal gradient might exist across the sample holder that would leave the region around the sample at a slightly different temperature than the region around the witness slide. Subsequent COMSOL simulations modeling the heating of the sample holder predicted a temperature difference of approximately 0.5°C between the sample and the witness slide so although the uncertainty in T_0 is relatively small, it is still illuminating to understand the effect that the background temperature has on the sample's response. Because the initial temperature of the sample determines the fraction of VO_2 domains that are in the metallic state before the pump is triggered, one would expect the sample's response to be sensitive to the value of T_0.

To study the effect of the background temperature, the simulation was run with a parametric sweep over T_0. For this and the following parameter studies, an incident intensity of 1.63×10^6 W/m^2 was used along with the optical properties of the plain VO_2 film. This value corresponds to the highest intensity for which experimental data is available, and this high value serves as a better testing ground for the various parameters since the additional incident energy transitions the VO_2 further along its SMT hysteresis. This ensures that the full range of dynamics in the VO_2's phase transition will be present in the simulation results. The background temperature T_0 was varied from 50°C to 60°C in steps of 2.5°C. Figure 9b shows that a 4.5% error in measuring the temperature can translate to as much as a 37% error in determining the maximum contrast. This sensitive dependence results from the steepness of the sigmoid governing the SMT. Figure 9c shows that 55°C sits right at the onset of sigmoid so a small variation in T_0 can translate into a large change in the final state of the sample.

Self-normalizing these contrast plots, it can be determined whether or not the background temperature contributes to the speed of the system response. Figure 9d shows that for lower values of T_0 the contrast drops more slowly to its maximum value, indicating that the background temperature does, in fact, have an effect on the system dynamics. This too can be understood

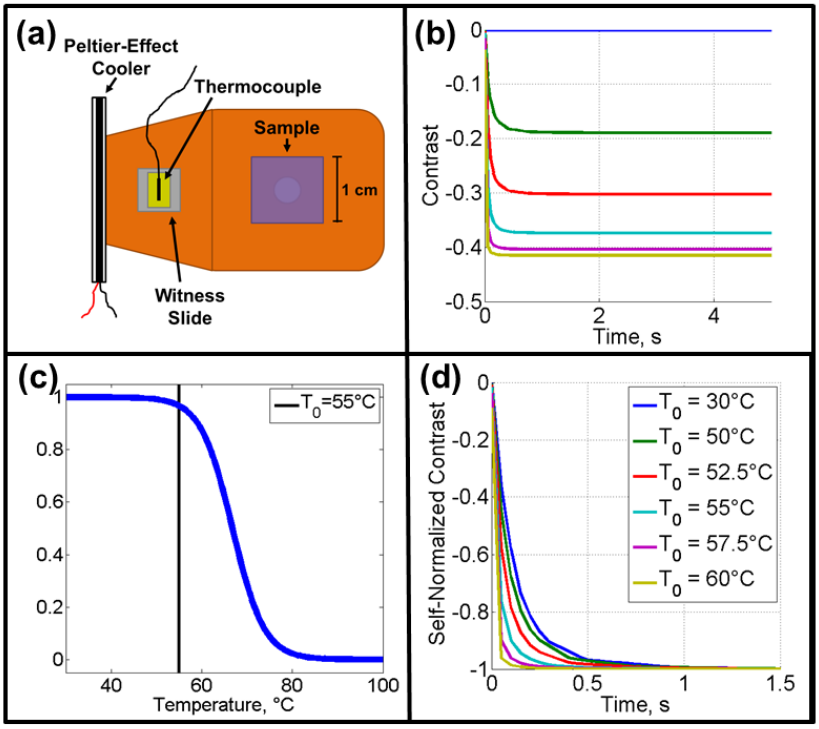

Figure 9. (a) The sample holder used in the experiments; (b) Contrast plotted as a function of time for five different background temperature values, T_0, and an incident intensity of 1.63×10^6 W/m^2; (c) Typical sigmoid mapping out the SMT of VO_2; (d) Heating dynamics for various values of T_0.

by analyzing the transition sigmoid of the VO_2 (Figure 9c). As T_0 decreases below 55°C, the system's initial point on the sigmoid is pushed into a region where the slope asymptotically approaches zero. In this region of small slope, the fraction of transitioned VO_2 grows more slowly as incident energy is pumped in. This results in the slowing of the transition that is observed in Figure 9d. The $T_0 = 30$°C line in this figure shows that this trend of slowing disappears as the temperature decreases past a certain point. This is because the local slope of the transition sigmoid governs the speed at which the contrast falls, and as T_0 continues to decrease, the second derivative of the sigmoid approaches zero so continued changes in T_0 affect very little changes in the system response. Physically, this corresponds to a situation where, even after the pump beam has contributed its energy, the temperature of the sample is still far enough below T_t that the VO_2 is still in the semiconducting state.

Another interesting question to investigate is whether the temperature dependence of the film's properties has any effect on the overall response of the system. To do this, the transitions governing the thermal and optical properties of the film were turned off in turn such that when the transitions for a certain property were turned off, the film retained the semiconducting values for that property throughout the simulation. Figure 10a shows clear evidence that the temperature dependence of the optical properties plays a much larger role than the temperature dependence of the thermal properties. In order to examine this further, the transitions of the

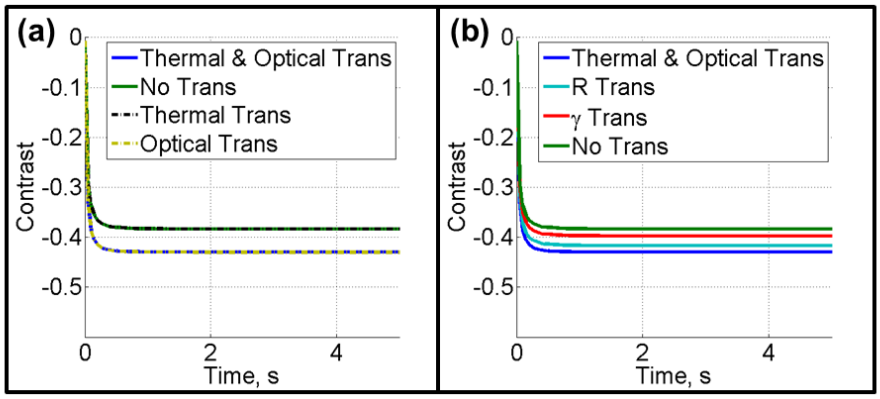

Figure 10. (a) Comparison of the contributions to the system response made by the transitions of the thermal and optical properties of the film for an incident intensity of 1.63×10^6 W/m^2; (b) Comparison of the contributions made by the various optical properties of the film.

two relevant optical properties (the reflectivity and the absorption constant) were turned off in turn. The results, shown in Figure 10b, show that the temperature dependence of the reflectivity makes the dominant contribution to the response of the sample. This can be understood by examining the percent change each constant undergoes as the VO_2 transitions. The reflectivity at 785 nm changes from 25% in the semiconducting state to 17% in the metallic, which corresponds to a 32% change in reflectivity. The absorption constant, however, changes by only 5.1%, from 5.8×10^{-3} nm^{-1} to 6.1×10^{-3} nm^{-1}. Thus, even though the heat source shows a stronger dependence on the absorption constant, the percent change in the absorption constant as the VO_2 transitions is small enough that its temperature dependence contributes less to the dynamics of the sample than the temperature dependence of the reflectivity.

That being said, it is interesting that the temperature dependence of the thermal properties of the film contribute so little to the dynamics of the system. The thermal conductance of the film undergoes a 66% change from 3.5 W/(m·K) to 5.8 W/(m·K), and the heat capacity changes by 20% from 645 J/(kg·K) to 774 J/(kg·K). Despite these large changes, the temperature dependences of the thermal properties contribute very little to the response of the system. This hints that the heating of the sample is largely independent of the thermal properties of the film since allowing the two relevant thermal parameters to change by as much as 66% and 20% over the course of the simulation had almost no visible effect on the results. This was verified by subsequent simulations where varying the metallic state thermal properties of the film by as much as 30% in either direction had almost no effect on the outcome of the simulations. From this the conclusion can be drawn that the heating of the sample is largely due to optical interactions within the film as opposed to thermal interactions. This corroborates the claim that the NPs act as 'nanoradiators' that scatter light back into the film and absorption centers that capture more incident energy, thus increasing the efficiency with which the film is heated. The light that is scattered by the NPs is subsequently absorbed by VO_2 interband transitions, while the light that is absorbed by the NPs is converted to heat via electron-phonon scattering and then transferred to the VO_2 by phonon-phonon scattering from the Au NP into the VO_2

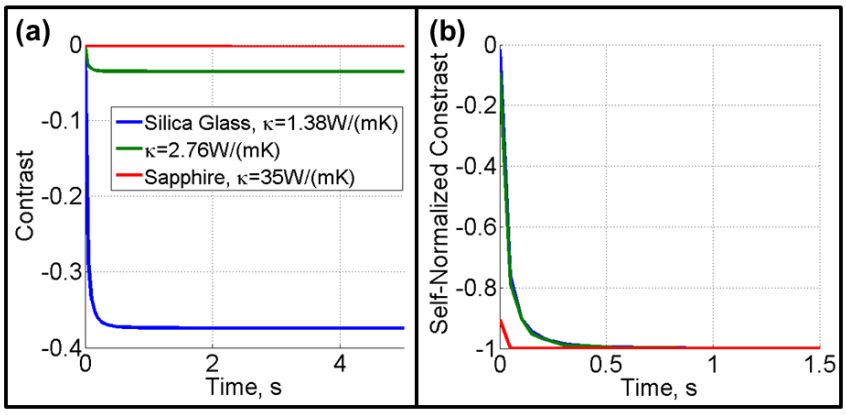

Figure 11. Study of the effect that the substrate thermal conductivity, κ, has on the (a) equilibrium contrast and (b) heating dynamics of the system for an incident intensity of 1.63×10^6 W/m^2.

film.[31] As calculated with Mie theory using the dipole approximation and assuming ellipsoidal NPs,[31] the ratio of the absorption cross-section to the scattering cross-section at $\lambda = 785$ nm is approximately 1.4. Because this ratio is close to unity, these two mechanisms should contribute almost equally to the heating of the film.

Although the thermal properties of the film have a relatively small effect on the response of the system, the thermal properties of the substrate are closely tied to the system's evolution. To show this, the thermal conductivity of the silica glass substrate was first doubled from 1.38 W/(m·K) to 2.76 W/(m·K), and then the silica glass substrate was replaced with one of sapphire (Al_2O_3) which has a thermal conductivity of 35 W/(m·K). The results, shown in Figure 11, show that the maximum contrast shows a strong, inverse relationship with the thermal conductivity of the substrate. In fact, with the sapphire substrate, the film temperature only rose 0.25°C (as compared to 22°C for the silica glass substrate) over the course of the simulation. Despite this strong dependence, however, the speed at which the contrast drops is largely unchanged by small changes in the thermal conductivity but is sped up drastically when the thermal conductivity of the substrate is increased by an order of magnitude as is the case for a sapphire substrate.

Because the temperature dependence of the reflectivity has such a large effect on the response of the system, one might guess that the reflectivity itself holds a fair amount of control over the system. To test this, the metallic state reflectivity was varied over a wide range (5% to 45%). Although lowering the metallic reflectivity from 45% to 5% did slightly slow the switching rate of the VO_2 (Figure 12a), these simulations seem to indicate that the reflectivity makes a more significant contribution to the maximum contrast than to the speed of the response (Figure 12b). The maximum contrast can be fit as a function of metallic state reflectivity with a linear relationship. This parallels the linear relationship of the heat source to the reflectivity (Equation 2) and matches what one would expect from the analytic expression for the temperature rise in the film,[31] thus lending support to the simulation since it is able to reproduce the trends predicted by theory.

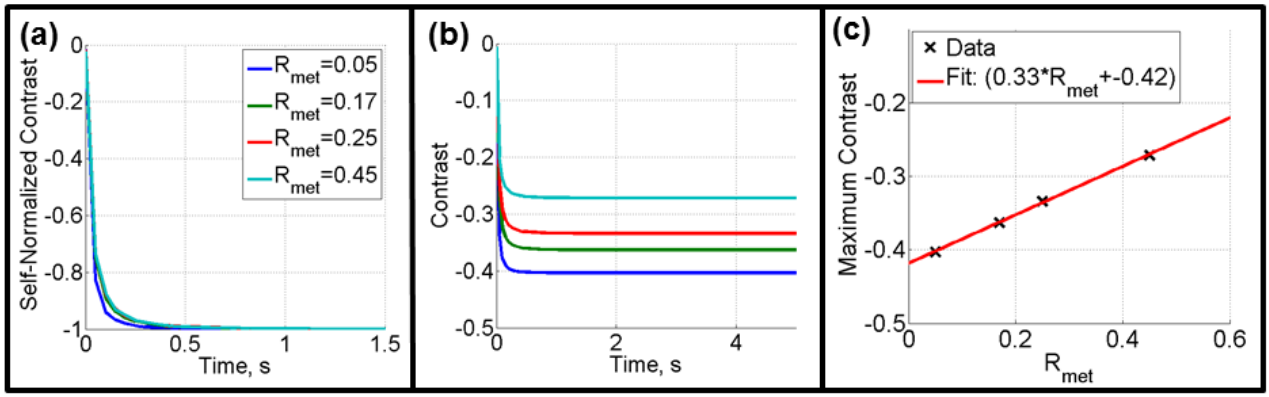

Figure 12. The (a) self-normalized and (b) normalized contrast for various values of R_{met} and an incident intensity of 1.63×10^6 W/m^2; (c) Equilibrium contrast plotted against values for the metallic state reflectivity and fit with a straight line.

Figure 4 showed that the nanocomposite responds very differently to the laser heating than the plain film. Since the only theoretical difference between the nanocomposite and the film is the absorption constant, one would hypothesize that the simulation is very sensitive to the absorption constant. To test this claim, the simulation was run with three different values for the metallic state absorption constant, γ_{met}. Figure 13a shows that a 30% change in the absorption constant can change the maximum contrast by as much as 21% with higher values producing larger maximum contrast. This effect is larger than the corresponding change in maximum contrast for different values of the metallic state reflectivity (10% increase for a 32% change in R_{met}), even though the temperature dependence of the reflectivity contributes more to the system dynamics than does the temperature dependence of the absorption constant. This is likely due to the increased sensitivity of the heat source to the absorption constant as opposed to the reflectivity.

Compared to the reflectivity, the speed of the sample's response also shows a stronger dependence on the absorption constant, with higher γ values increasing the speed of the transition as the incident heat is absorbed more efficiently. Neither the absorption constant nor the reflectivity has as much of an effect on the speed of the response as does the background temperature T_0, though, which seems to have the most control over how quickly the system equilibrates. By varying γ_{met}, it was shown that increasing the absorption constant both increases the maximum contrast and reduces the time to equilibrium. Figure 4 shows that switching from the plain film to the nanocomposite has the same two effects, thus supporting the treatment of the nanocomposite as a plain VO_2 film with an increased effective absorption constant.

After studying the effects of the various simulation parameters, it becomes easier to interpret any differences between experiment and simulation which may reveal heretofore unthought-of aspects of the system dynamics. The simulation was run with an incident intensity of 1.20×10^6 W/m^2 for both the plain film and nanocomposite, and this was compared to the experimental data for the corresponding intensity (Figure 14a). The simulation calculates the maximum contrast fairly well, especially in the case of the nanocomposite, but it fails to predict

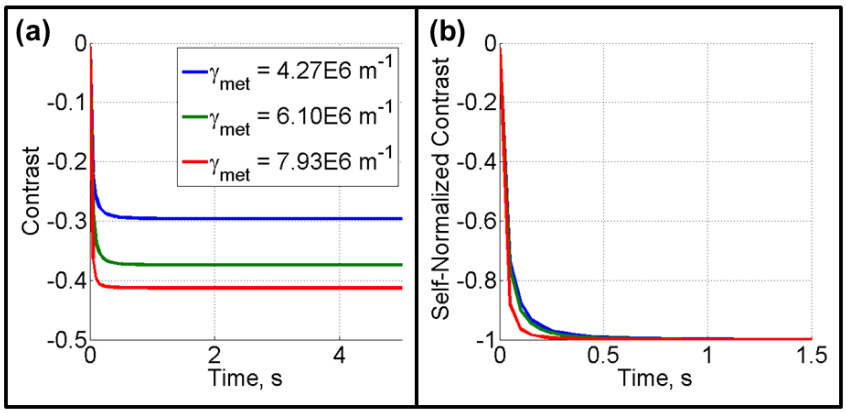

Figure 13. The (a) contrast and (b) self-normalized contrast for three values of the metallic state absorption constant γ_{met} and an incident intensity of 1.63×10^6 W/m^2.

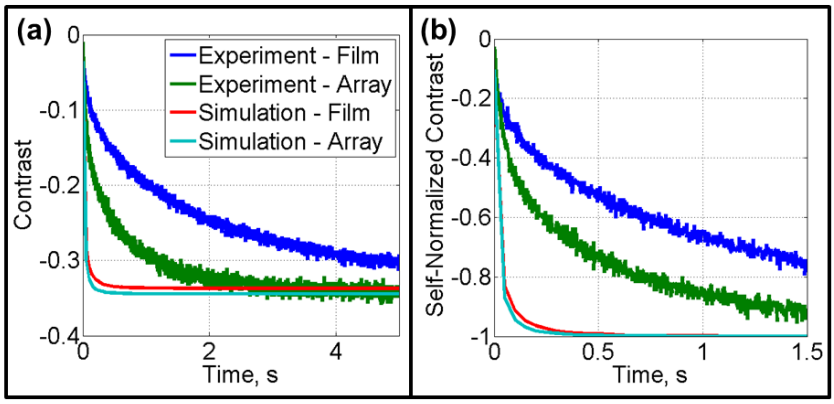

Figure 14. (a) Contrast and (b) self-normalized contrast plots of experimental and simulation results for $I_0 = 1.20 \times 10^6$ W/m^2.

the speed at which the system reaches that maximum contrast. The rate at which the contrast falls is much quicker in the simulation than in the experiment, but the contrast falls more quickly on the array than off in each case so the general trends are preserved. The parameter study described earlier showed that there could be many reasons why the maximum contrast achieved in simulation does not agree with the experimental values for the plain film case. The exact values of the background temperature, reflectivity, and absorption constant all directly affect the maximum contrast that the simulation predicts so any errors in the values used for these parameters would translate into errors in the predicted maximum contrast.

The increased speed of the system response in the simulation is harder to account for, however. Of the parameters studied, only the background temperature was able to slow the system response by a sizeable amount, but this slowing leveled off at a response speed that was still much too slow at a background temperature that was unrealistically low ($\approx$ 30°C). The reflectivity and absorption constants both had small effects on the speed, but neither was close to enough to correct the observed discrepancy. This suggests that either there is some aspect of

the experiment that is not being accounted for in the simulation or some simulation parameter that has not yet been examined contributes to the system response.

4. CONCLUSIONS AND FUTURE DIRECTIONS

Finite element analysis was performed on Au::VO_2 nanocomposites and plain VO_2 films. It was determined that the temperature dependence of the optical properties affects the system more than the changes that occur in the thermal properties as the VO_2 undergoes its SMT. Within these optical properties, the temperature dependence of the reflectivity contributes more to the response of the sample than does the temperature dependence of the absorption constant. This dominance of the reflectivity temperature dependence lies in contrast to the more sensitive dependence that the system shows to the specific values of the absorption constant than to the specific values of the reflectivity. That being said, perhaps the most pertinent parameter is, in fact, the background temperature, which is sensitively coupled to both the equilibrium contrast and the speed at which that contrast is achieved. The thermal properties of the film and the thermal contact resistance at the interface between the film and substrate were both determined to have minimal effects on the system response, lending support to the claim that the nanocomposites heat the film more efficiently by acting as both nanoradiators and absorption centers.

Comparisons of experimental results to simulation showed fairly good agreement in maximum contrast but large discrepancies in the speed of the system response. The small maximum contrast discrepancies can be understood through the possibility of errors in the estimated properties of the sample, while the discrepancies in the speed of the system can only be partially explained in this way. This suggests that either something is missing from the simulation or that the parameter study overlooked some important aspect of the simulation. One candidate for the former is the thin ITO layer that coats the silica glass substrate. It is reasonable to think that this thin layer would contribute to the system response, but it was not accounted for in the simulation due to a lack of reliable material constants for ITO. Some possible parameters that have not yet been tested include the thickness of the film, the beam spot size, and the properties of the film in its semiconducting state. Each of these aspects of the simulation could feasibly contribute to the heating dynamics of the sample and should be pursued in future investigations.

The finite element simulations performed here have advanced the understanding of Au::VO_2 nanocomposites and their response to low-powered laser heating. As more progress is made on understanding why these structures respond as they do to laser heating, it will become easier to fabricate a nanocomposite with a given set of desired properties, which is important if these structures are ever to be used as optical switches, protective coatings, or optical limiting materials.

ACKNOWLEDGMENTS

This work was supported by the U.S. Department of Energy, Office of Science (DE-FG02-01ER45916), the ITT Corporation's National Security Technology Applications Division, and

the generous support of a William and Nancy McMinn Honor Scholarship for the Natural Sciences. Thanks to Davon Ferrara for guidance throughout the research process and Joyeeta Nag for assistance with VO_2 fabrication.

REFERENCES

1. F. J. Morin, "Oxides which show a metal-to-insulator transition at the Neel temperature," *Physical Review Letters* **3**, pp. 34–36, 1959.
2. A. Cavalleri, M. Rini, H. H. W. Chong, S. Fourmaux, T. E. Glover, P. A. Heimann, J. C. Kieffer, and R. W. Schoenlein, "Band-selective measurements of electron dynamics in VO_2 using femtosecond near-edge x-ray absorption," *Physical Review Letters* **95**, p. 067405, 2005.
3. C. Kübler, H. Ehrke, R. Huber, R. Lopez, A. Halabica, R. F. Haglund, Jr., and A. Leitenstorfer, "Coherent structural dynamics and electronic correlations during an ultrafast insulator-to-metal phase transition in VO_2," *Physical Review Letters* **99**, p. 116401, 2007.
4. J. Y. Suh, R. Lopez, L. C. Feldman, and R. F. Haglund, Jr., "Semiconductor to metal phase transition in the nucleation and growth of VO_2 nanoparticles and thin films," *Journal of Applied Physics* **96**, p. 1209, 2004.
5. K. Okimura, Y. Sasakawa, and Y. Nihei, "X-ray diffraction study of electric field-induced metal-insulator transition of vanadium dioxide film on sapphire substrate," *Japanese Journal of Applied Physics* **45**, pp. 9200–9202, 2006.
6. W. Wang, Y. Luo, D. Zhang, and F. Luo, "Dynamic optical limiting experiments on vanadium dioxide and vanadium pentoxide thin films irradiated by a laser beam," *Applied Optics* **45**(14), pp. 3378–3381, 2006.
7. S. Chen, H. Ma, X. Yi, T. Xiong, H. Wang, and C. Ke, "Smart VO_2 thin film for protection of sensitive infrared detectors from strong laser radiation," *Sensors and Actuators A* **115**, pp. 28–31, 2004.
8. M. Soltani, M. Chaker, E. Haddad, R. V. Kruzelesky, and D. Nikanpour, "Optical switching of vanadium dioxide thin films deposited by reactive pulsed laser deposition," *Journal of Vacuum Science and Technology A* **22**(3), pp. 859–864, 2004.
9. M. Soltani, M. Chaker, E. Haddad, and R. Kruzelesky, "1×2 optical switch devices based on semiconductor-to-metallic phase transition characteristics of VO_2 smart coatings," *Measurement Science and Technology* **17**, pp. 1052–1056, 2006.
10. S. A. Maier, *Plasmonics: Fundamentals and Applications*, Springer Science+Business Media, LLC, New York, NY, 2007.
11. U. Kreibig and M. Vollmer, *Optical Properties of Metal Clusters*, Springer-Verlag, Berlin, 1995.
12. C. F. Bohren and D. R. Huffman, *Absorption and Scattering of Light by Small Particles*, Wiley-Interscience, New York, 1983.
13. B. K. Canfield, S. Kujalal, K. Jefimovs, T. Vallius, J. Turunen, and M. Kauranen, "Polarization effects in the linear and nonlinear optical responses of gold nanoparticle arrays," *Journal Of Optics A-Pure And Applied Optics* **7**, pp. S110–S117, 2005.
14. C. Tabor, R. Murali, M. Mahmoud, and M. A. El-Sayed, "On the use of plasmonic nanoparticle pairs as a plasmon ruler: The dependence of the near-field dipole plasmon coupling on nanoparticle size and shape," *Journal of Physical Chemistry A* **113**, pp. 1946–1953, 2008.

15. P. K. Jain, W. Huang, and M. A. El-Sayed, "On the universal scaling behavior of distance decay of plasmon coupling in metal nanoparticle pairs: A plasmon ruler equation," *Nano Letters* **7**, pp. 2080–2088, 2007.
16. P. K. Jain and M. A. El-Sayed, "Noble metal nanoparticle pairs: Effect of medium for enhanced sensing," *Nano Letters* **8**, pp. 4347–4352, 2008.
17. P. Olk, J. Renger, M. T. Wenzel, and L. M. Eng, "Distance dependent spectral tuning of two coupled metal nanoparticles," *Nano Letters* **8**, pp. 1174–1178, 2008.
18. C. L. Haynes, A. D. McFarland, L. Zhao, R. P. V. Duyne, G. C. Schatz, L. Gunnarsson, J. Prikulis, B. Kasemo, and M. Käll, "Nanoparticle optics: The importance of radiative dipole coupling in two-dimensional nanoparticle arrays," *Journal of Physical Chemistry B* **107**, pp. 7337–7342, 2003.
19. B. Lamprecht, G. Schider, R. T. Lechner, H. Ditlbacher, J. R. Krenn, A. Leitner, and F. R. Aussenegg, "Metal nanoparticle gratings: Influence of dipolar particle interaction on the plasmon resonance," *Physical Review Letters* **84**, pp. 4721–4724, 2000.
20. M. W. Knight, Y. Wu, J. B. Lassiter, and P. Nordlander, "Substrates matter: Influence of an adjacent dielectric on an individual plasmonic nanoparticle," *Nano Letters* **9**(5), pp. 2188–2192, 2009.
21. P. K. Jain, X. Huang, I. H. El-Sayad, and M. A. El-Sayed, "Review of some interesting surface plasmon resonance-enhanced properties of noble metal nanoparticles and their applications to biosystems," *Plasmonics* **3**, pp. 107–118, 2007.
22. J. Y. Suh, E. U. Donev, D. W. Ferrara, K. A. Tetz, L. C. Feldman, and R. F. Haglund, Jr., "Modulation of gold particle-plasmon resonance by the metal-semiconductor transition of vanadium dioxide," *Journal of Optics A: Pure and Applied Optics* **10**, p. 055202, 2008.
23. D. W. Ferrara, J. Nag, E. MacQuarrie, K. Appavoo, and R. F. Haglund, Jr., "Far-field coupling in arrays of gold and gold::vanadium dioxide nanodimers," *Proceedings of SPIE* **7394**, p. 73942Q, 2009.
24. M. Maaza, O. Nemraoui, C. Sella, A. C. Beye, and B. Baruch-Barak, "Thermal induced tunability of surface plasmon resonance in $AuVO_2$ nano-photonics," *Optics Communications* **254**, pp. 188–195, 2005.
25. G. Xu, Chun-Ming, P. Jin, M. Tazawa, and D.-M. Chen, "Nano-Ag on vanadium dioxide. I. localizaed spectrum tailoring," *Journal of Applied Physics* **104**, p. 053101, 2008.
26. G. Xu, Chun-Ming, M. Tazawa, P. Jin, and D.-M. Chen, "Nano-Ag on vanadium dioxide. II. thermal tuning of surface plasmon resonance," *Journal of Applied Physics* **104**, p. 053101, 2008.
27. G. Xu, C.-M. Huang, M. Tazawa, P. Jin, D.-M. Chen, and L. Miao, "Electron injection assisted phase transition in a nano-Au-VO_2 junction," *Journal of Applied Physics* **104**, p. 053101, 2008.
28. G. Xu, C.-M. Huang, M. Tazawa, P. Jin, and L.-H. Chen, "Tunable optical properties of nano-Au on vanadium-dioxide," *Optics Communications* **282**, pp. 896–902, 2009.
29. D. W. Ferrara, E. R. MacQuarrie, A. B. Kaye, and R. F. Haglund, Jr., "Plasmon-enhanced low-intensity laser switching of gold::vanadium dioxide nanocomposites," *Submitted to Applied Physics Letters* , 2011.
30. D.-W. O. . C. K. . S. R. . D. Cahill, "Thermal conductivity and dynamic heat capacity across the metal-insulator transition in thin film VO_2," *Applied Physics Letters* **96**, 2010.
31. D. Ferrara, *Plasmonic Interactions Within Gold::Vanadium Dioxide Hybrid Structures*. PhD thesis, Vanderbilt University, 2010.